A large scale multi-fluid/dispersed phase approach for spray generation in aeronautical fuel injectors

Ghislain Blanchard, Davide Zuzio, Philippe Villedieu

A large scale multi-fluid/dispersed phase approach for spray generation in aeronautical fuel injectors

Ghislain Blanchard[1], **Davide Zuzio**[1], **Philippe Villedieu**[1]
[1] *ONERA, The French Aerospace Lab*
2 avenue Edouard Belin 31055 Toulouse, France
davide.zuzio@onera.fr
ghislain.blanchard@onera.fr
philippe.villedieu@onera.fr

Abstract

Atomization is usually neglected in industrial numerical simulations of aeronautical combustors, despite the increasing physical fidelity of the LES approaches. The reason comes from the strong multi-scale nature of the problem: the typical space and time lengths are too small for their resolution to be afforded. The influence of the atomization process should however be taken in account when simulating unsteady processes like ignition and combustion instabilities. This work proposes a large scale numerical methodology (LSS, Large Scale Simulation) to simulate the unsteady assisted atomization process in industrial simulations of combustion chambers. The LSS approach involves a two-fluid resolution for the first stages of primary atomization and a dynamic local transfer of the liquid phase to a dispersed phase solver. An atomization model generates volume source terms for the multi-fluid solver which remove the liquid mass, while acting as an advanced adaptive injector for the dispersed phase solver. The methodology has been successfully tested on a planar sheared liquid sheet.

Keywords: two-fluid model, dispersed phase, multi-scale, atomization modelling

1. Introduction

In aircraft combustion chambers the injection of fuel is mostly achieved by air-blast atomizers. These devices are meant to pulverize a liquid jet, sheet or thin film with the shearing effect of an incoming high-speed airflow. The numerical simulation of this process is challenging in reason of its strong multi-scale aspect, where several order of magnitude separate the physical phenomena, from the primary atomization of the liquid jet to the formation and evolution of the small droplets. Several studies have been devoted to the development of numerical simulation methods for dealing with this problem. The methods based on the sharp interface methods aim to describe the whole atomization process, from the larger scales to the smaller ones ([1], [2], [3]). More ambitious multi-scale approaches include multi-scale adaptive techniques coupled with a local resolved two-phase DNS for the liquid atomization ([4], [5],[6], [7], [8], [9]). However, their objective remains to directly simulate atomization up to the smallest scale.

In contrast to these works, the objective of the proposed approach is to develop a numerical method allowing the resolution of the larger scale phenomena of the liquid fragmentation mechanism as well as the spray formation and evolution in the context of more industrial-oriented simulations. Three numerical tools are used to achieve this goal:

- a separate phases approach, based on a finite volume discretization of conservation equations for both liquid and gas phases, considered as compressible fluids. This will be referred as the two-fluid model;
- a dispersed phase solver, specifically a Lagrangian solver which allows the simulation of the droplet cloud carried by the gas flow;
- an additional sub-scale atomization model. The model is able to detect zones where the droplets are most likely to appear and to act subsequently as an advanced numerical injector, transferring the resolved liquid to an appropriate distribution of numerical droplets. Taking in account the instabilities of the injection, it gives more accurate initial position and velocity of each particle. The model naturally respects the resolved liquid core and performs the conversion at realistic break-up lengths.

The first point is detailed in [10]. This paper focuses mainly on the third point, the sub-scale transition model between the two-phase solvers.

2. Two-fluid model

The two-fluid model considers two non miscible compressible fluids assumed to be simultaneously present at any point in space. The two fluids are supposed to be in local mechanical equilibrium, having locally the same velocity and the same pressure, in a four-equation model:

$$\boldsymbol{v} = \boldsymbol{v}_l = \boldsymbol{v}_g \tag{1}$$

$$p = p_l = p_g \tag{2}$$

The mass and momentum balance equations of the model lead to the system:

$$\frac{\partial \tilde{\boldsymbol{\rho}}}{\partial t} + div\left(\tilde{\boldsymbol{\rho}} \otimes \boldsymbol{v}\right) = 0 \tag{3}$$

$$\frac{\partial \rho \boldsymbol{v}}{\partial t} + div\left(\rho \boldsymbol{v} \otimes \boldsymbol{v} + p\mathbf{I}\right) = div\left(\boldsymbol{\tau}_v + \boldsymbol{\tau}_c\right) + \rho \boldsymbol{g} + \boldsymbol{s}_p \tag{4}$$

with $\tilde{\boldsymbol{\rho}} = [\alpha_l \rho_l,\ \alpha_g \rho_g]^T = [\tilde{\rho_l},\ \tilde{\rho_g}]^T$ the bulk densities, $\alpha_{l,g}$ the volume fractions of the liquid and the gas, $\rho_{l,g}$ the bulk densities of the liquid and the gas, $\boldsymbol{\tau}_c$ and $\boldsymbol{\tau}_v$ respectively the capillary and viscous stress tensor, $\boldsymbol{g}$ the gravity acceleration and $\boldsymbol{s}_p$ the two-way coupling source term. The mixture density is $\rho = \alpha_l \rho_l + \alpha_g \rho_g$. In system (3) + (4) it is worth noting that both fluids play a symmetric role and that the volume fraction of one

of the two-phase, e.g. α, is not a primary unknown but rather an outcome of the model given by the closure relationship, resulting from the assumption of local mechanical equilibrium (2):

$$\begin{cases} \rho_g \left(\tilde{\rho}_g/\alpha_g^*\right) = \rho_l \left(\tilde{\rho}_l/\alpha_l^*\right) \\ \alpha_l^* + \alpha_g^* = 1 \end{cases} \tag{5}$$

given the equations of state for each phase k:

$$p_k = p_{0,k} + c_k^2 \left(\rho_0 - \rho_{0,k}\right) \tag{6}$$

The choice of the (6) EOS (where c is the speed of sound) is justified by the assumption that density changes are considered as negligible in the low-Mach regimes of the considered applications. The fluid mixture is supposed to behave as a Newtonian fluid for which the general form of the viscous stress tensor reads:

$$\boldsymbol{\tau}_v = -\frac{2}{3}\mu \, div(\boldsymbol{v})\mathbf{I} + \mu \left(\nabla \boldsymbol{v} + {}^t \nabla \boldsymbol{v}\right) \tag{7}$$

where $\mu = \alpha_l \mu_l + \alpha_g \mu_g$ is the dynamic viscosity of the two fluids mixture. The capillary stress tensor is modelled according to the Continuum Surface Stress (CSS) formulation [6] which is well suited to diffuse interface method and which is conservative by construction.

$$\boldsymbol{\tau}_c = \sigma \left[\mathbf{I} - \frac{\nabla\alpha_l \otimes \nabla\alpha_l}{\|\nabla\alpha_l\|^2}\right] \|\nabla\alpha_l\| \tag{8}$$

The numerical resolution of the system (3)+(4) is assured by a partially implicit finite volume scheme on unstructured 3D meshes. An implicit time discretization of the mass conservation equations avoids the acoustic CFL limitation of the time step [11]. A second-order MUSCL scheme is used to achieve robust second order space accuracy, while a special attention has been paid to the multidimensional slope limitation procedure in order to limit the smearing of the interface [12]..

3. Dispersed phase model

The spray is modelled with a statistical dispersed phase approach. It is based on the resolution of the scalar function $f^{(p)}$ representing the average liquid droplets density. At a given time, the number of droplets of radius $[r, r+\delta r]$ moving at a velocity in the interval $[v, v+\delta v]$ is given by $f^{(p)}(t, \boldsymbol{x}_p, \boldsymbol{v}_p, r_p) d\boldsymbol{x}_p d\boldsymbol{v}_p dr_p$. The underlying hypothesis on the dispersed phase are the following:

- the droplets are spherical and rigid
- the volume occupied by the droplet is small (diluted spray)
- the influence of the turbulence small scales is neglected

The evolution of the function $f^{(p)}$ is given by

$$\frac{\partial}{\partial t}\left(f^{(p)}\right) + \nabla_x \left(\boldsymbol{v}_p f^{(p)}\right) + \nabla_v \left(\frac{F_p}{m_p} f^{(p)}\right) = 0 \tag{9}$$

with F_p the external forces acting on the particles and $m_p = 4/3 \; \rho_p \pi r_p^3$ the particle mass (ρ_p being the liquid density). The external forces F_p acting on the particles are the aerodynamic drag force $F_{p,d}$ and the gravity force $F_{p,g}$. The expressions are the following:

$$F_{p,d} = \frac{1}{2}\rho_{f@p} \, \pi r_p^2 C_D \|\boldsymbol{v}_{f@p} - \boldsymbol{v}_p\| \left(\boldsymbol{v}_{f@p} - \boldsymbol{v}_p\right) \tag{10}$$

$$F_{p,g} = m_p \, \boldsymbol{g} \tag{11}$$

where $\rho_{f@p}$ and $\boldsymbol{v}_{f@p}$ are respectively the density and the velocity of the carrier phase at the particle location $\boldsymbol{x}_p$ and C_d the drag coefficient. From [13], the drag coefficient is :

$$C_D(Re_p) = \begin{cases} 24(1 + 0.15 Re_p^{0.687}) Re_p^{-1} & \text{if } Re_p < 1000 \\ 0.445 & \text{otherwise} \end{cases} \tag{12}$$

with

$$Re_p = 2 \, r_p \rho_g \|\boldsymbol{v}_{f@p} - \boldsymbol{v}_p\| \mu_g^{-1} \tag{13}$$

By defining a characteristic relaxation time in the form

$$\tau_p = \frac{4 \rho_p d_p}{3 \, C_D(Re_p) \rho_g \|\boldsymbol{v}_{f@p} - \boldsymbol{v}_p\|} \tag{14}$$

the drag force acting on the particle can be written as

$$F_{p,d} = m_p \left(v_{f@p} - v_p\right) \tau_p^{-1} \tag{15}$$

The spray is coupled to the carrier phase in a full two-way coupling. The numerical discretization of equation (9) is done by a Lagrangian method, where volume-less numerical parcels carry the information of an arbitrary number of physical droplets. This number is referred to as numerical weight $w_{p,k}$ of the parcel k. The time evolution of the N_p parcels is determined by the following equations:

$$\forall k \in [1, N_p], \begin{cases} \dfrac{d}{dt}(\boldsymbol{x}_{p,k}) = \boldsymbol{v}_{p,k} \\ \dfrac{d}{dt}(\boldsymbol{v}_{p,k}) = \left(\boldsymbol{v}_{f@p} - \boldsymbol{v}_p\right) \tau_{p,k}^{-1} + \boldsymbol{g} \\ w_{p,k}(t) = w_{p,k}(0) \end{cases} \tag{16}$$

The coupling source term $\boldsymbol{s}_p$ appearing in the momentum equation (4) reads

$$\boldsymbol{s}_p = \sum_{k=1}^{N_p} -w_{p,k} F_{p,k} \delta\left(\boldsymbol{x} - \boldsymbol{x}_{p,k}(t)\right) \tag{17}$$

A fractional step integration in performed with the systems (3)+(4) and (16). More details about the numerical integration are available in [12].

4. Large Scale coupling model

The multi-scale approach proposed in this work is meant to provide a high quality droplet injection obtained by the time-resolved simulation of primary atomization by the multi-fluid solver, and then by employing an atomization model to dynamically generate the droplets. The multi-fluid solver has been successfully in capturing the main features of the primary atomization of a two dimensional planar liquid sheet [10].

In this paper, the coupling model will be referred to as the "atomization model" for the sake of simplicity. The model should assure the transfer and the compatibility of the information from one solver (and from one scale) to another. The first issue is that the two-fluid solver is based on a continuous formulation, while the dispersed phase solver is based on a Lagrangian (discrete) formulation. To overcome this issue, the model is based on a set of new variables storing the informations needed for the coupling, which communicate with the two solvers via appropriate source terms. These variables will employ the lower-case $[\cdot]_a$ or the upper-case$[\cdot]^a$. This way, the two solvers can coexist in all the domain, the coupling taking action where particular conditions are met.

4.1. *General model*

The system (4)+(3) can be rewritten in a compact form :

$$\frac{\partial \boldsymbol{w}}{\partial t} + \nabla \cdot \mathcal{H} + \nabla \cdot (\mathcal{C} + \mathcal{V}) + \boldsymbol{s}_g + \boldsymbol{s}_d + \boldsymbol{s}_{a \leftarrow s} \tag{18}$$

where $\boldsymbol{s}_d$ is the particles drag term and $\boldsymbol{s}_{a \leftarrow s}$ the atomization coupling source term. The system (16) is modified by new "injection conditions":

$$\begin{cases} \dfrac{d}{dt}(\boldsymbol{x}_{p,k}) = \boldsymbol{v}_{p,k} \\ m_p \dfrac{d}{dt}(\boldsymbol{v}_{p,k}) = F_{drag} + \boldsymbol{g} \\ + \text{injection conditions depending on } s_{d \leftarrow a} \end{cases} \tag{19}$$

The model variables are defined as $\boldsymbol{w}_{atom} =^t (\rho_a, (\rho \boldsymbol{v})_a)$, following an evolution in the general form

$$\frac{\partial}{\partial t}(\boldsymbol{w}_a) = \boldsymbol{s}_{s \to a} + \boldsymbol{s}_{d \to a} \tag{20}$$

with $\boldsymbol{s}_{s \to a}$ and $\boldsymbol{s}_{d \to a}$ the terms modelling the exchanges from respectively the separate phases and the dispersed phase model towards the atomization model.

4.2. *Mass source terms, two-fluid towards model*

The source term $\boldsymbol{s}_{s \to a} =^t \left(s_{s \to a}^{(\rho)_a}, s_{s \to a}^{(\rho \boldsymbol{v})_a} \right)$ include the terms for the mass flow rate and the relative momentum which are transferred from the two-fluid model to the atomization model. The mass flux rate is written as:

$$s_{s \to a}^{(\rho)_a} = \tilde{\rho}_l \nu_a \mathcal{R}_a \tag{21}$$

where $\tilde{\rho}_l$ is the liquid mass in the two-fluid model, ν_a an atomisation frequency (or $\nu_a^{-1} = \tau_a$ a characteristic atomization time) and $\mathcal{R}_a$ an activation function determining whether the model is active or not. The atomization frequency corresponds to a physical droplet generation rate. No well-established model is able to predict this value. In the proposed strategy the model should use local resolved quantities. The shearing effect on the sheet being the atomization energy source, the local vorticity of the velocity field can be an indicator of the intensity of the breakup:

$$\nu_a = \|\nabla \times \boldsymbol{v}\| \tag{22}$$

The activation term $\mathcal{R}_a$ is responsible for the general behaviour of the model, and it should respect several conditions:

- the atomization should occur where the two-fluid solution is too smeared
- the model should not affect resolved liquid structures
- the droplets should not be generated "upwind" of a resolved structure [1]

The resulting function has been written as:

$$\mathcal{R}_a = \chi_a(\alpha_l, \nabla \alpha_l)\, \psi_a(\nabla \alpha_l, \boldsymbol{v}) \tag{23}$$

The χ_a function depends on the local liquid volume fraction and its gradient, its function is to activate the model by respecting the first and second point above-mentioned.

$$\chi_a(\alpha_l, \nabla \alpha_l) = \begin{cases} 1 & \text{if } \alpha_l \leq \alpha_l^a \text{ and } \|\nabla \alpha_l\| \leq \|\nabla \alpha_l\|^a \\ 0 & \text{otherwise} \end{cases} \tag{24}$$

where α_l^a and $\|\nabla \alpha_l\|^a$ are threshold values for respectively the volume fraction and its gradient in the two-fluid model (they are constant values set at the beginning of the simulation). The constant α_l^a determines the cells where a small volume of fluid is present: a value of $\alpha_l^a = 0.1$ is a good compromise, as it allows to generate the droplets near the break-up point as well as producing a dispersed phase sufficiently diluted. The term $\|\nabla \alpha_l\|$ is directly related to the thickness of the interface:

$$\delta_{interface} \approx \|\nabla \alpha_l\|^{-1} \tag{25}$$

Low values of this gradient depict a zone where the interface is smeared, where the liquid is fragmenting into structures too small to be tracked by the two-fluid model. Conversely, high values describe the perimeter of a well-resolved structure even if the local α_l is small. Its value being limited for a theoretical sharp interface by $\|\nabla \alpha_l\|_{\max} \cdot \Delta x = 1$, the retained value for practical purposes is $\|\nabla \alpha_l\|^a = C_{\|\nabla \alpha_l\|} \Delta x$, with $C_{\|\nabla \alpha_l\|} = 0.5$.

The ψ_a function contains geometrical considerations. It is defined as:

$$\psi_a(\nabla \alpha_l, \boldsymbol{v}) = \max\left(0, \cos(\theta_a)\right) \tag{26}$$

θ_a being the angle between the local interface normal (pointing from the liquid to the gas) and the local two-fluid velocity vector:

$$\cos(\theta_a) = -\frac{\nabla \alpha_l \cdot \boldsymbol{v}}{\|\nabla \alpha_l\|\, \|\boldsymbol{v}\|} \tag{27}$$

Its function is to respect the third point, which is allowing the model to produce droplets mostly where the normal vector is aligned to the velocity vector. Three scenarios can be distinguished by this function:

(a) the interface normal is perpendicular to the local velocity vector. This corresponds to a pure shearing effect of the gas on the liquid. In the targeted applications the pure tearing of droplets is almost never observed, so that the production of droplets is minimized in this case[2].

(b) the interface normal and the local velocity vector are aligned. This case represents the situation where the stretching of the liquid and the ligament mechanism are active, so the droplet production is fully authorized here.

(c) the interface normal and the local velocity vector are opposite. This represents an upwind face of a resolved structure, no atomization is allowed in this case.

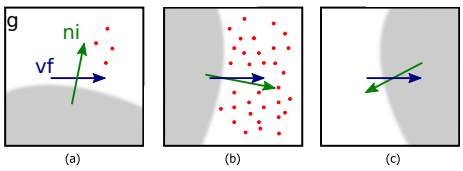

Figure 1: Effect of the ψ_a function, based on the interface geometry and the local two-fluid velocity.

4.3. *Momentum source terms, two-fluid towards model*

When the mass is transferred from the two-fluid model to the model, the momentum carried by the liquid is transferred as well in order to assure global conservation. A negative term appears in equation 4 to balance the two-way coupling with the particles. This term depends on the mass source term in equation (21) :

$$\boldsymbol{s}_{s \to a}^{(\rho \boldsymbol{v})_a} = \boldsymbol{s}_{s \to a}^{(\rho)_a} \boldsymbol{v} = \tilde{\rho}_l \nu_a \mathcal{R}_a \boldsymbol{v} \tag{28}$$

[1] As they would travel inside a liquid structure, which would be at odd with the dispersed phase hypothesis

[2] In liquid propulsion injectors, where the gas velocities can attain 300 $m.s^{-1}$, the tearing effect is important: the psi_a function is different in these applications

The velocity used in (28) should be the liquid velocity: however, in the 4 equation model only one velocity is available in each cell. Further developments will be devoted to find a better approximation of $\boldsymbol{v}_l$. Since $\rho_l \gg \rho_g$, this approximation is acceptable as it implies $\alpha_l \gg 1/\left(1+\rho_l/\rho_g\right) \approx 10^{-3}$ respected by the threshold $\alpha_l^a = 0.1$ of equation (24). Within the discretization of equations (21) and (28), at each time-step each cell cumulates the quantities into the $\boldsymbol{w}_a$ vectors following equation (20).

4.4. Mass and momentum source terms, model towards two-fluid

The source terms seen by the two-fluid solver are defined by global conservation as:

$$s_{a\to s}^{(\tilde{\rho}_l)_a} = -s_{s\to a}^{(\rho)_a} \tag{29}$$

$$\boldsymbol{s}_{a\to s}^{(\rho\boldsymbol{v})_a} = -\boldsymbol{s}_{s\to a}^{(\rho\boldsymbol{v})_a} \tag{30}$$

Equation (29) and (30) are respectively related to the liquid mass and the global momentum equations.

4.5. Pressure conservation

An important step for the removal of the liquid in the two-fluid solver is necessary in order to avoid pressure fluctuations. A sudden gas expansion is expected in the newly created empty volume freed by the liquid, as the dispersed phase solver does not take in account the volume of the droplets. A constant pressure condition is imposed, $dp_l = dp_g = 0 \Longleftrightarrow d\rho_l = d\rho_g = 0$. This implies

$$d\tilde{\rho}_l = \rho_l d\alpha_l \tag{31}$$

$$d\tilde{\rho}_g = \rho_g d\alpha_g = \rho_g d\left(1-\alpha_l\right) = -\rho_g d\alpha_l \tag{32}$$

and then

$$d\tilde{\rho}_g = -\frac{\rho_g}{\rho_l} d\tilde{\rho}_l \tag{33}$$

Equation (33) means that a mass source term has to be imposed in the gaseous phase equation to "fill" the volume freed by the extracted liquid:

$$s_{a\to s}^{(\tilde{\rho}_g)_a} = -(\rho_g/\rho_l) s_{a\to s}^{(\tilde{\rho}_l)_a} = (\rho_g/\rho_l) s_{s\to a}^{(\rho)_a} \tag{34}$$

Exact conservation for the gas mass is lost; however, the high density ratio between the phases implies a very low added mass to the system. Moreover, the volume ratio between the injected liquid and gas in aeronautical injectors is small. The momentum source term (30) is updated in consequence:

$$\boldsymbol{s}_{a\to s}^{(\rho\boldsymbol{v})} = -\left(1-\rho_g/\rho_l\right)\tilde{\rho}_l \nu_a \mathcal{R}_a \boldsymbol{v} \tag{35}$$

4.6. Mass and momentum source terms, dispersed phase towards model

The mass subtracted from the two-fluid model is temporarily stored into the model variables $\boldsymbol{w}_a$. Without any constraint from the discrete model of the dispersed phase solver, at each time-step the mass could be directly injected in form of a numerical droplet:

$$\boldsymbol{s}_{d\to a} = -\boldsymbol{s}_{s\to a} \tag{36}$$

so that $\boldsymbol{w}_a = \text{const}$. However, the droplet characteristic formation time (dependent on equation (22)) is likely to be larger than the regular time-step. This would imply the generation of a far too large number of droplets, with numerical weights largely inferior to the unity. Instead, using system (20) allows to store the particle mass until the desired numerical weight is attained: the injection characteristic time becomes independent of the two-fluid time-step and the atomization rate. The number of droplet $N_{p,inj}|_i$ injected in the cell Ω_i at the time-step $\left[t^n, t^{n+1}\right[$ is then defined as the biggest integer number satisfying the following condition:

$$m_a - N_{p,inj}|_i m_p^{(num)} \geq 0 \tag{37}$$

where m_a is the total liquid mass contained in the model variables:

$$m_a = \int_{\Omega_i} \rho_a\left(t^{n+1}, \boldsymbol{x}\right) dx \tag{38}$$

and $m_p^{(num)} = m_p w_p$ the user-defined mass of the numerical particle. In each cell, the atomization model source terms reads:

$$s_{d\to a}^{(\rho)_a} = -\frac{1}{|\Omega_i|} N_{p,inj}|_i m_p^{(num)} \delta\left(t-t^{n+1}\right) \tag{39}$$

$$s_{d\to a}^{(\rho\boldsymbol{v})_a} = -\frac{1}{|\Omega_i|} N_{p,inj}|_i m_p^{(num)} \boldsymbol{v}_a \delta\left(t-t^{n+1}\right) \tag{40}$$

where the model velocity at $t = t^{n+1}$ is given by

$$\boldsymbol{v}_a = (\rho\boldsymbol{v})_a/(\rho)_a \tag{41}$$

Equations (39) and (40) mean that each time a droplet is injected, its mass and momentum are subtracted from the model variables $\boldsymbol{w}_a$.

4.7. Droplets injection

Once the source terms (39) and (40) are defined, the numerical droplets are injected in each affected cell Ω_i by respecting:

- the number of injected particles is $N_{p,inj}|_i$
- the initial velocity of each droplet is $\boldsymbol{v}_a$
- the initial position is randomly taken inside Ω_i
- the properties of the droplets are the same as the liquid
- the diameter of the droplets is a user-defined parameter at the present time

5. Assisted atomization of a liquid sheet

The multi-scale methodology has been applied to the simulation of the primary atomization of a liquid sheet sheared by two co-flowing air streams. In this configuration, the sheet-shape is unstable: hydrodynamic instabilities are the source of the atomization mechanisms and determine the primary break-up characteristics. Two different moments can be distinguished [14], [15]. In the primary atomization, the sheet becomes subject to longitudinal instabilities, which are the results of the shearing effect: Kelvin-Helmholtz instabilities perturb the plane sheet, starting a sinusoidal stream-wise oscillation all along the sheet. Then, fully three dimensional instabilities generate transverse modulations. The sheet breaks into smaller liquid packs, ligaments and bag-like structures. This continuous fragmentation ends with the formation of the spray of droplets.

5.1. Numerical set-up

The considered numerical configuration aims to reproduce a simple atomization device as the one experimentally investigated in [16]. The injector consists of a NACA-shaped injector $89\ mm$ long, immersed into a channel airflow, discharging the liquid by a rectangular fence $a = 300\ \mu m$ thick. The liquid used in the reference experience is water. In the present work, the two air ducts are $9\ mm$ thick at each side of the injector. The velocity V_{air} is the maximum air velocity at this location. Room conditions, $T_0 \approx 300\ K$ and $P_0 = 1\ bar$, are supposed.

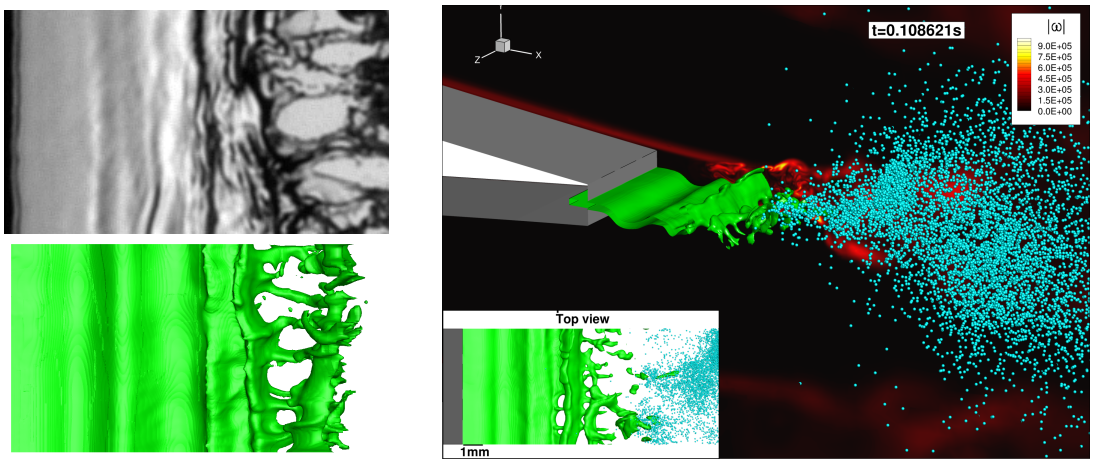

(a) (b)

Figure 2: Results of the planar liquid sheet atomization. (a) Visual comparison of the experience (top) and the simulation (bottom) (b) Fully developed atomization with the atomization model in action. In green the two-fluid model resolved liquid ($\alpha_l = 0.5$ iso-contour), in cyan the Lagrangian droplets. From [12].

Dimensional parameters			
Air velocity	V_{air}	80	$m.s^{-1}$
Water velocity	V_{water}	2.2	$m.s^{-1}$
Air density	$\rho_{0,air}$	1.225	$kg.m^{-3}$
Water density	$\rho_{0,water}$	1000	$kg.m^{-3}$
Air viscosity	$\mu_{0,air}$	$1.8\ 10^{-5}$	$Pa.s$
Water viscosity	$\mu_{0,water}$	$1\ 10^{-3}$	$Pa.s$
Surface tension	σ	0.072	$N.m^{-1}$

Table 1: Test case parameters, dimensional.

The chosen physical parameters are typical of a "stretched ligament" break-up, where the primary atomization manifests in the form of membranes and longitudinal ligaments formation. The momentum ratios involving the "stretched ligament" break-up are comprised between $0.5 < M < 4$ (from [15] and [17]). The parameters are summarized in tables 1 and 2[3]. The numerical three-dimensional domain, depicted in figure 3, includes the channel, the injector and a vast chamber in which the sheet atomization occurs without confinement effects. The mesh consists of about 15 M elements extruded in the transverse direction. The mesh includes a Cartesian zone refined around the liquid inlet, where the sheet breaks-up. The cell size is here $\Delta x_{fine} = 30\ \mu m$. The droplet diameter has been fixed at $d_{drop} = 100\ \mu m$.

Non-dimensional parameters	
Air Reynolds (Re_δ)	4900
Water Reynolds (Re_a)	366
Momentum flow rate	1.61
Weber (We_a)	31

Table 2: Test case parameters, non dimensional parameters.

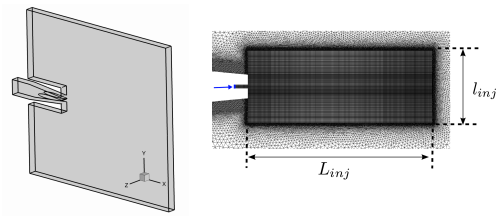

Figure 3: Numerical domain and local mesh.

5.2. *Results*

A snapshot of the simulation is depicted in figure 2. The sheet has already attained its steady oscillation regime. The two-fluid model captures the stream-wise oscillation as well as the transverse modulations which induce the break-up. It is able do capture the atomization process up to the formation of the ligaments, as shown in the comparison 2(a). The atomization model is active and correctly performs the coupling after the break-up point, 2(b). The droplets evolves following their initial velocities and the drag force induced by the airflow.

Two macroscopic quantities have been measured, the global oscillation frequency and the mean break-up length. The results are summarized in table 3 in comparison with the experimental values of [16]. The results are in quite good agreement with the experiences, despite a slight overestimation of both values.

In order to evaluate the effect of the atomization model, three more two dimensional simulations have been performed on the same configuration, where the air velocity has been set respectively to 30, 50 and 80 $m.s^{-1}$. Figure 4 shows the droplet distribution in the three cases, as well as the time averaged droplet volume fraction $< \alpha_p >$. The averaged fields clearly show a decrease in the spray opening with increased airflow, correctly following the different sheet spatial evolution in the difference regimes. A comparison with the experiences is difficult to perform because of the difficulty to employ the same criterion for the visualizations and the simulations.

[3]The $Re_{air,\delta}$ is based on the boundary layer thickness; the $Re_{water,a}$ and the We_a on the liquid sheet thickness.

	Simulation	Experience
Oscillation frequency [Hz]	664	574
Break-up length [mm]	7.85	5.42

Table 3: Quantitative liquid sheet characteristics, simulation and experience.

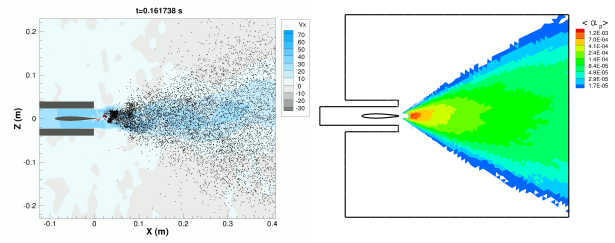

(a) $V_{gas} = 30\ m.s^{-1}$

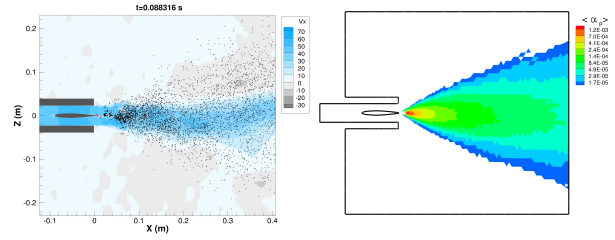

(c) $V_{gas} = 50\ m.s^{-1}$

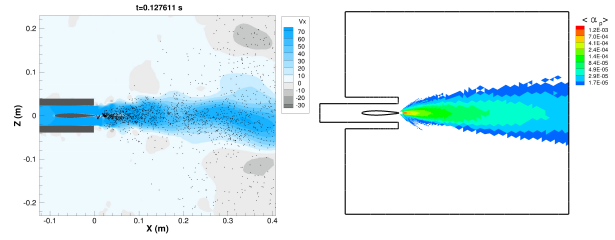

(e) $V_{gas} = 80\ m.s^{-1}$

Figure 4: Snapshots of the two-dimensional simulations with different air velocities, atomisation model activated. (Left) Instantaneous fields and (right) mean particle density $< \alpha_p >$.

6. Conclusion

A new approach is proposed for the simulation of the assisted atomization. This involves coupling of two types of models. The first one, called two-fluid model, is based on the Navier-Stokes equations for two immiscible compressible fluids. It is used to describe the largest scales of the atomization mechanism in the near-injector area. The second one, called spray model, is based on a dispersed phase approach. This model describes the evolution of the droplet cloud produced by the primary fragmentation of liquid jet. The coupling of these two models has been achieved by introducing an atomization model which ensure liquid transfer between the two-fluid model and the spray model. Special care has been taken in order to assure a robust coupling. The approach has been applied to the numerical simulation of a three dimensional sheared liquid sheet: comparison with experimental data have shown that the presented methodology gives promising results.

References

[1] R. Lebas, T. Menard, P. Beau, A. Berlemont, F. Demoulin, Numerical simulation of primary break-up and atomization: Dns and modelling study, International Journal of Multiphase Flow 35 (2009) 247–260.

[2] M. Gorokhovski, M. Herrmann, Modeling primary atomization, Annual Review of Fluid Mechanics 40 (2008) 343–366.

[3] O. Desjardin, V. Moureau, H. Pitsch, An accurate conservative level set/ghost fluid method for simulating turbulent atomization., Journal of Computational Physics 227 (18) (2008) 839–Ű–8416.

[4] M. Herrmann, The influence of density ratio on the primary atomization of a turbulent liquid jet in crossflow, Proceedings of the Combustion Institute 33 (2011) 2079–2088.

[5] G. Tomar, D. Fuster, S. Zaleski, S. Popinet, Multiscale simulations of primary atomization using gerris, Computers and Fluids 39 (10) (2010) 1864–1874.

[6] G. Pau, J. Bell, A. Almgren, K. Fagnan, M. Lijewski, An adaptive mesh refinement algorithm for compressible two-phase flow in porous media, Computational Geosciences 16 (3) (2012) 577–592. doi:10.1007/s10596-011-9270-2.

[7] M. Sussman, A parallelized, adaptive algorithm for multiphase flows in general geometries, Computers and Structures 83 (6-7) (2005) 435–444.

[8] S. Popinet, An accurate adaptive solver for surface tension driven interfacial flows., Journal of Computational Physics 228 (2009) 5838–5866.

[9] D. Zuzio, J.-L. Estivalezes, An efficient block parallel amr method for two phase flow simulations, Computer and Fluids 44 (2011) 339–357.

[10] G. Blanchard, P. Villedieu, D. Zuzio, Numerical simulation of primary atomization of a sheared liquid sheet, 25th ILASS, Crete, 2013.

[11] N. Grenier, P. Villedieu, J.-P. Vila, An accurate low-mach scheme for a compressible two fluid model applied to sloshing phenomena., in: Proceedings of ASME-JSME-KSME Joint Fluids Engineering Conference 2011 AJK2011-FED July 24-29, Hamamatsu, Shizuoka, Japan, 2011.

[12] G. Blanchard, Modélisation et simulation multiéchelle de l'atomisation d'une nappe liquide cisaillée., Ph.D. thesis, ISAE (2014).

[13] L. Schiller, Z. Naumann, A drag coefficient correlation, Ver. Deutsch. Ing. (1935) 77–318.

[14] B. Stapper, W. Sowa, G. Samuelsen, An experimental study of the effects of liquid properties on the breakup of a two-dimensional liquid sheet., Journal of Engineering for Gas Turbines and Power 1 (114) (1992) 32–39.

[15] A. Mansour, N. Chigier, Disintegration of liquid sheets., Physics of Fluids A: Fluid Dynamics 2 (1990) 706–719.

[16] B. Déjean, P. Berthoumieu, P. Gajan, Experimental study on the influence of liquid and air boundary conditions on a planar air-blasted liquid sheet, International Journal of Multiphase Flow 79 (2016) 202 – 213. doi:http://dx.doi.org/10.1016/j.ijmultiphaseflow.2015.09.002.

[17] A. Lozano, F. Barreras, G. Hauke, C. Dopazo, Longitudinal instabilities in a air-blasted liquid sheet., Journal of Fluid Mechanics 437 (2001) 143–173.